Electronic Supplementary Material (ESI) for Journal of Materials Chemistry C.

$Ca_2YScAl_2Si_2O_{12}:Cr^{3+}$ phosphor-in-glass film for laser-driven high-power near-infrared lighting

Yi Lin,[a,c] Gaoming Dong,[a,c] Hang Lin,[*c,d] Bo Wang,[e] Pengfei Wang,[d] Ju Xu,[d] Yao Cheng,[d] Yan Xiong,[b] Yuansheng Wang[*d]

[a] College of Chemistry, Fuzhou University, Fuzhou, Fujian, 350002, China.

[b] Hubei Provincial Key Laboratory of Green Materials for Light Industry, Hubei University of Technology, Wuhan, Hubei, 430068, China

[c] State Key Laboratory of Structural Chemistry, Fujian Institute of Research on the Structure of Matter, Chinese Academy of Sciences, Fuzhou, Fujian, 350002, China.

[d] Fujian Key Laboratory of Nanomaterials, Fujian Institute of Research on the Structure of Matter, Chinese Academy of Sciences, Fuzhou, Fujian, 350002, China.

[e] School of Applied Physics and Materials, Wuyi University, Jiangmen, Guangdong, 529020, China.

E-mail: lingh@fjirsm.ac.cn; Tel/Fax: +86-591-63179423
E-mail: yswang@fjirsm.ac.cn; Tel/Fax: +86-591-63179438

Supplementary Note S1:

All decay curves of Cr^{3+} ions can be fitted with a double-exponential function:[1]

$$I_t = I_0 + A_1 \exp\left(\frac{-t}{\tau_1}\right) + A_2 \exp\left(\frac{-t}{\tau_2}\right) \#(S1)$$

$$\tau^* = \frac{A_1\tau_1^2 + A_2\tau_2^2}{A_1\tau_1 + A_2\tau_2} \#(S2)$$

where I_t and I_0 are the luminescence intensity and the initial intensity at $t = 0$, respectively; A_1 and A_2 are constants; τ_1 and τ_2 are the decay times for fast and slow exponential components, respectively; and τ^* is the average fluorescence decay time.

The τ^* changes obviously with the monitor wavelength, indicating more than one emission centers. The decay curves are well fitted with a double-exponential function, indicating that the existence of two emitting centers.

Supplementary Note S2:

The corresponding crystal field parameters for Cr^{3+} can be calculated by using the following formulas proposed by Henry, Tanabe, and Sugano:[2-4]

$$10D_q = E\left({}^4A_{2g} \rightarrow {}^4T_{2g}\right) - \Delta S/2 \#(S3)$$

$$D_q/B = \frac{15\left(\Delta E/D_q - 8\right)}{\left(\Delta E/D_q\right)^2 - 10\left(\Delta E/D_q\right)} \#(S4)$$

$$\Delta E = E\left({}^4A_{2g} \rightarrow {}^4T_{1g}\right) - E\left({}^4A_{2g} \rightarrow {}^4T_{2g}\right) \#(S5)$$

$$\Delta S = E\left({}^4A_{2g} \rightarrow {}^4T_{2g}\right) - E\left({}^4T_{2g} \rightarrow {}^4A_{2g}\right) \#(S6)$$

where D_q and B are the crystal field splitting energy and Racah parameter, respectively. The values of E (${}^4A_{2g} \rightarrow {}^4T_{1g}$) and E (${}^4A_{2g} \rightarrow {}^4T_{2g}$) are calculated from the corresponding peak energy of the excitation band, and ΔE represents the energy difference between these two energy levels. The stokes shift ΔS is calculated from the peak position of the PLE spectrum corresponding to E (${}^4A_{2g} \rightarrow {}^4T_{2g}$) and the peak position in the PL spectrum corresponding to E (${}^4T_{2g} \rightarrow {}^4A_{2g}$).

Selecting the peak energy of $^4A_{2g} \rightarrow {}^4T_{2g}$ (15949 cm^{-1}), peak energy of $^4A_{2g} \rightarrow {}^4T_{1g}$ (22989 cm^{-1}) and peak energy of $^4T_{2g} \rightarrow {}^4A_{2g}$ (12422 cm^{-1}), ΔE, ΔS and D_q were calculated to be 7040 cm^{-1}, 3527 cm^{-1} and 1418.55 cm^{-1}, respectively. Therefore, the value of D_q/B representing the strength of the crystal field was calculated to be 1.82 $<$ 2.3, which demonstrates Cr^{3+} locates in a weak crystal field, leading to broadband emission. Furthermore, on the basis of negligible change in peak position of $^4A_{2g} \rightarrow {}^4T_{2g}$ and $^4A_{2g} \rightarrow {}^4T_{1g}$ under different detection wavelengths (Fig. S2), selecting the peak energy of Cr(1):$^4T_{2g} \rightarrow {}^4A_{2g}$ (12579 cm^{-1}) and the peak energy of Cr(2):$^4T_{2g} \rightarrow {}^4A_{2g}$ (11377 cm^{-1}), the calculated Dq/B values for Cr(1) and Cr(2) were 1.84 and 1.71, respectively, supporting the fact that the Cr(2) dodecahedral site has weaker crystal field strength than the Cr(1) octahedral site.

Table S1. Comparisons made on luminescence performance parameters of several Cr^{3+}-doped garnet-type phosphors (λ_{em} > 800 nm).[5-13]

Hosts	λ_{ex} (nm)	λ_{em} (nm)	IQE (%)	I_{423K}/I_{298K}	FWHM (nm)	Refs.
$La_3Sc_2Ga_3O_{12}$	490	818	35	≈75	145	5
$Ca_4ZrGe_3O_{12}$	477	840	35	≈38	160	6
$Ca_3Y_2Ge_3O_{12}$	460	800	81	\	≈76	7
$Ca_2LuScGa_2Ge_2O_{12}$	465	800	\	59	150	8
$Ca_2LuGa_3Ge_2O_{12}$	460	803	\	89.5	267	9
$Ca_2LaZr_2Ga_{2.8}Al_{0.2}O_{12}$	450	820	58.3	≈64	160	10
$Mg_3Y_2Ge_3O_{12}$	436	811	\	\	226	11
$Gd_3Zn_{0.8}Ga_{3.4}Ge_{0.8}O_{12}$	449	800	79.6	40.2	202	12
$Gd_3Zn_2GaGe_2O_{12}$	≈460	852	\	\	211	12
$Ca_2LuScAl_2Si_2O_{12}$	442	752/804	73.7	76	142	13
$Ca_2YScAl_2Si_2O_{12}$	435	805	63	60	165	This work

Table S2. Comparisons made on NIR output power of several NIR pc-LD devices fabricated with Cr^{3+}-doped fluorescent conversion materials.[14-21]

Compounds	NIR output power	Categories	Refs.
$Gd_3Al_2Ga_3O_{12}:Cr^{3+}$	1652.6 mW@5.5 W	ceramic	14
$Y_3Al_5O_{12}$-$Al_2O_3:Cr^{3+}$	≈1400 mW@10.7 W	ceramic	15
$BaMgAl_{10}O_{17}:Cr^{3+}$	3.4 mW@100 mW	PiG	16
$MgO:Cr^{3+}/Ni^{2+}$	5.3 mW/mm^2	PiGF	17
$MgO:Cr^{3+}$	6360 mW	ceramic	18
$Gd_3Sc_2Al_3O_{12}:Cr^{3+}$	484.34 mW@2.3 A	ceramic	19
$Ca_3Sc_2Si_3O_{12}:Ce^{3+}/Cr^{3+}/Li^{+}$	1697 mW@22 W/mm^2	PiGF	20
$CaLu_2Mg_2Si_3O_{12}:Ce^{3+},Cr^{3+},Nd^{3+}$	1218 mW@17 W(21.7 W/mm^2)	PiGF	21
$Ca_2YScAl_2Si_2O_{12}:Cr^{3+}$	2626 mW@17W(21.7W/mm^2)	PiGF	This work

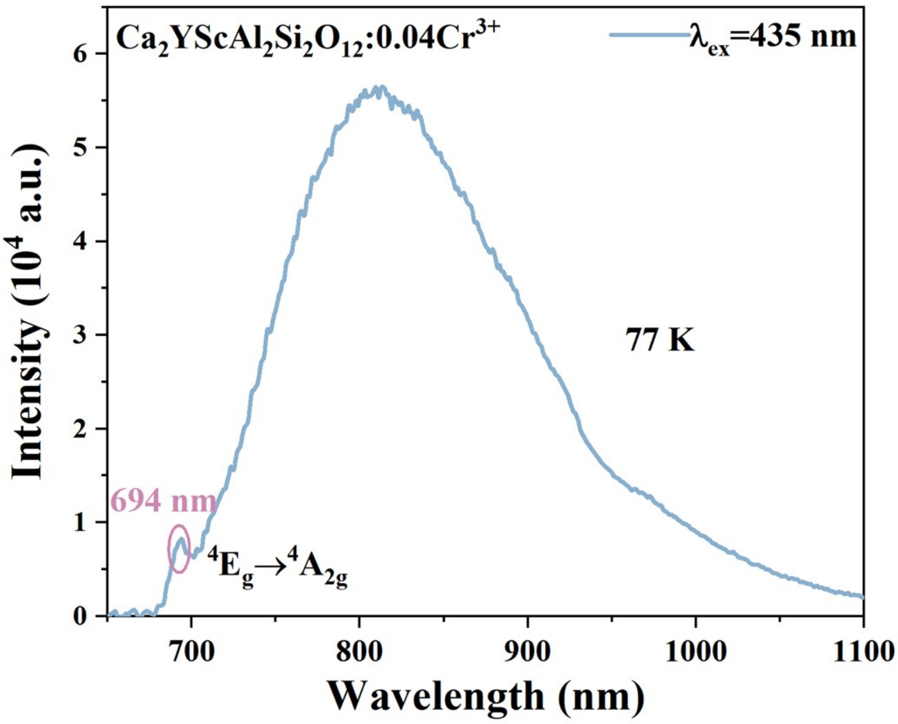

Fig. S1. PL spectrum of CYSAS:$0.04Cr^{3+}$ phosphor at 77 K.

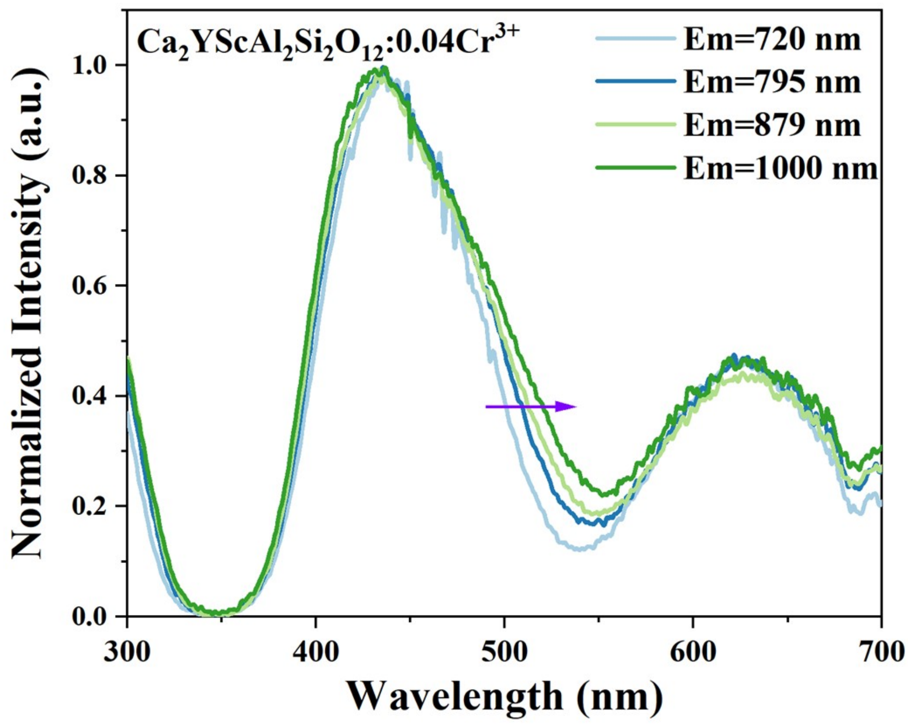

Fig. S2. Normalized PLE spectra of CYSAS:0.04Cr^{3+} phosphor at different detection wavelengths.

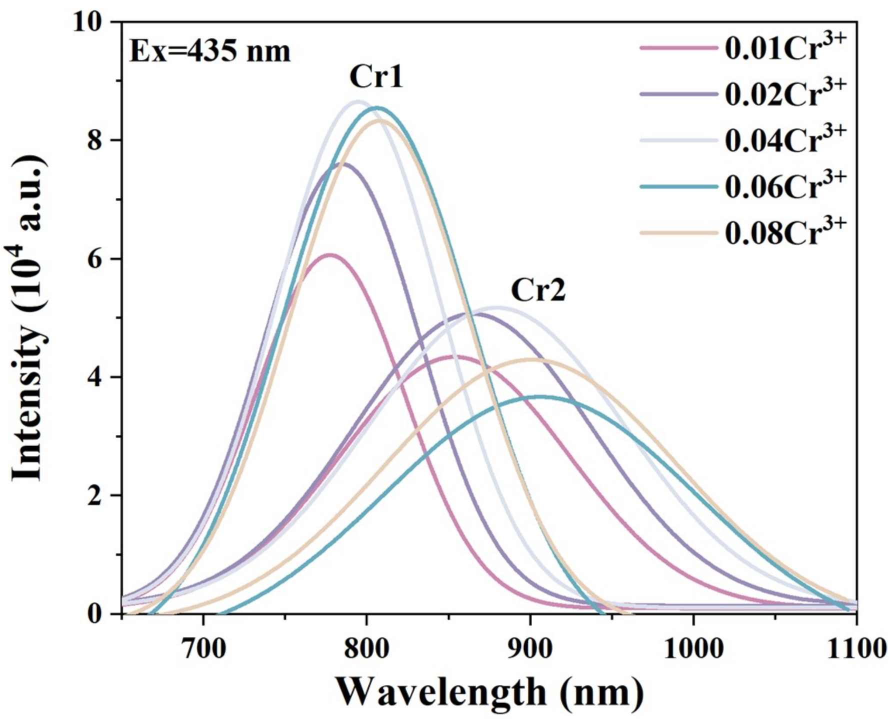

Fig. S3. Cr(1) and Cr(2) spectra fitted by a Gaussian function of CYSAS:yCr^{3+} (y = 0.01-0.08) phosphors.

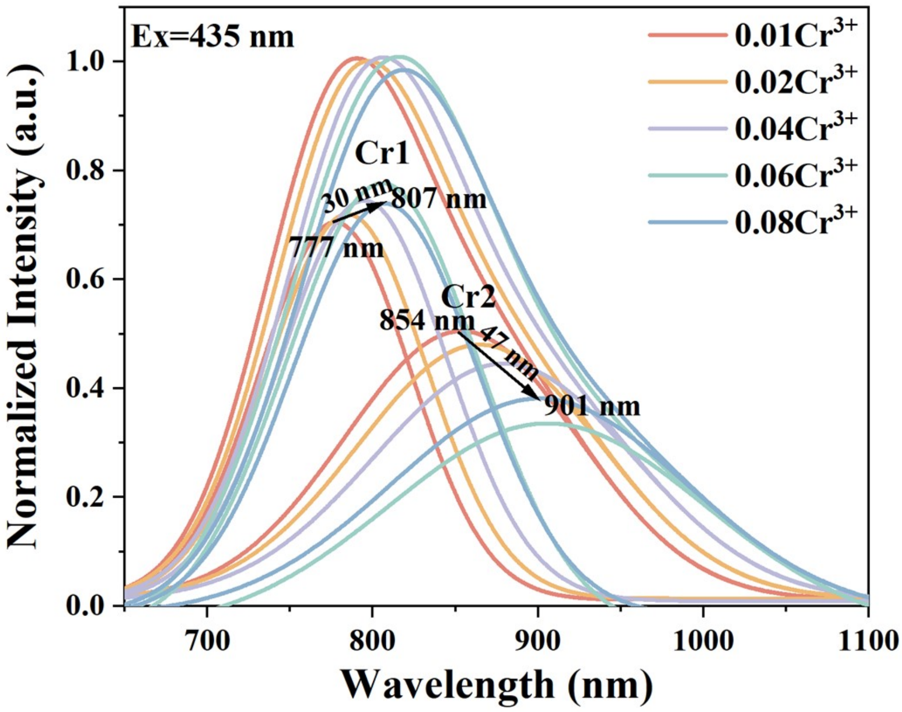

Fig. S4. Normalized PL spectra (including Cr(1) and Cr(2) spectra fitted by a Gaussian function) of CYSAS:yCr^{3+} (y = 0.01-0.08) phosphors.

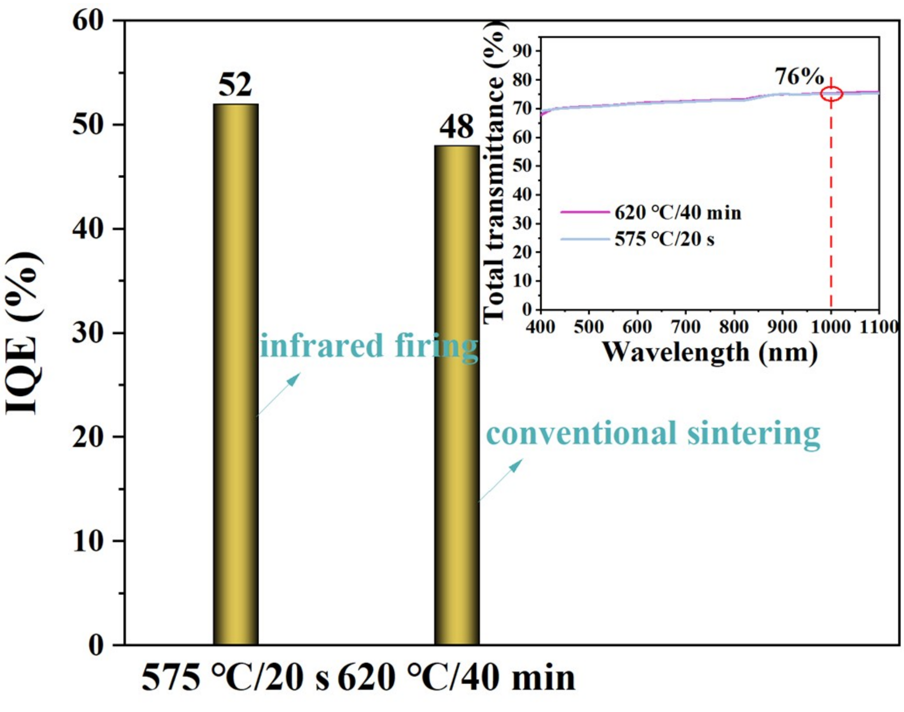

Fig. S5. IQE comparisons made on the CYSAS:0.04Cr^{3+} PiGF-on-SP samples prepared employing a rapid infrared firing technique and a conventional thermal annealing method, respectively; the inset shows transmittance spectra (400-1100 nm) of bare glass films fabricated by using these two sintering processes.

References

1. S. H. Miao, Y. J. Liang, Y. Zhang, D. X. Chen and X. J. Wang, *ACS Appl. Mater. Interfaces*, 2021, **13**, 36011-36019.
2. R. Y. Li, Y. F. Liu, C. X. Yuan, G. Leniec, L. J. Miao, P. Sun, Z. H. Liu, Z. H. Luo, R. Dong and J. Jiang, *Adv. Opt. Mater.*, 2021, **9**, 2100388.
3. A. Trueba, P. Garcia-Fernandez, J. M. García-Lastra, J. A. Aramburu, M. T. Barriuso and M. Moreno, *J. Phys. Chem. A*, 2011, **115**, 1423-1432.
4. C. X. Yuan, R. Y. Li, Y. F. Liu, L. L. Zhang, J. H. Zhang, G. Leniec, P. Sun, Z. H. Liu, Z. H. Luo, R. Dong and J. Jiang, *Laser Photon. Rev.*, 2021, **15**, 2100227.
5. B. Malysa, A. Meijerink and T. Jüstel, *J. Lumines.*, 2018, **202**, 523-531.
6. J. M. Xiang, J. M. Zheng, X. Q. Zhao, X. Zhou, C. H. Chen, M. K. Jin and C. F. Guo, *Mat. Chem. Front.*, 2022, **6**, 440-449.
7. N. Mao, S. Q. Liu, Z. Song, Y. Yu and Q. L. Liu, *J. Alloy. Compd.*, 2021, **863**, 158699.
8. B. Bai, P. P. Dang, D. Y. Huang, H. Z. Lian and J. Lin, *Inorg. Chem.*, 2020, **59**, 13481-13488.
9. T. C. Lang, M. S. Cai, S. Q. Fang, T. Han, S. S. He, Q. Y. Wang, G. H. Ge, J. Wang, C. Z. Guo, L. L. Peng, S. X. Cao, B. T. Liu, V. I. Korepanov, A. N. Yakovlev and J. B. Qiu, *Adv. Opt. Mater.*, 2022, **10**, 2101633.
10. Y. Liu, S. He, D. Wu, X. L. Dong and W. P. Zhou, *ACS Appl. Electron. Mater.*, 2022, **4**, 643-650.
11. X. Y. Meng, X. S. Zhang, X. L. Shi, K. L. Qiu, Z. J. Wang, D. W. Wang, J. X. Zhao, X. Li, Z. P. Yang and P. L. Li, *RSC Adv.*, 2020, **10**, 19106.
12. Y. Wang, Z. J. Wang, G. H. Wei, Y. B. Yang, S. X. He, J. H. Li, Y. W. Shi, R. Li, J. W. Zhang and P. L. Li, *Chem. Eng. J.*, 2022, **437**, 135346.
13. Y. Jin, Z. Zhou, R. X. Ran, S. Tan, Y. F. Liu, J. J. Zheng, G. T. Xiang, L. Ma and X. J. Wang, *Adv. Opt. Mater.*, 2022, **10**, 2202049.
14. H. J. Jiang, L. Y. Chen, G. J. Zheng, Z. H. Luo, X. H. Wu, Z. H. Liu, R. Y. Li, Y. F. Liu, P. Sun and J. Jiang, *Adv. Opt. Mater.*, 2022, **10**, 2102741.
15. G. J. Zheng, W. G. Xiao, H. J. Wu, J. H. Wu, X. F. Liu and J. R. Qiu, *Laser Photon. Rev.*, 2021, **15**, 2100060.
16. L. You, R. D. Tian, T. L. Zhou and R. J. Xie, *Chem. Eng. J.*, 2021, **417**, 129224.
17. S. M. Gu, B. M. Liu, S. C. Si and J. Wang, *J. Mater. Chem. C*, 2023, **11**, 9014-9022.
18. G. C. Liu, W. B. Chen, Z. Xiong, Y. Z. Wang, S. Zhang and Z. G. Xia, *Nat. Photonics*, 2024, **18**, 562-568.
19. Y. L. Ma, C. Y. Shao, L. Wu, X. C. Li, Y. Tian, L. W. Zeng, L. L. Lu, B. Q. Zhang, Z. C. Wang, X. Z. Chen, D. B. Xue, G. X. Jiang, Y. B. Hui, S. Q. Chen and D. Q. Chen, *Ceram. Int.*, 2024, **50**, 26624-26633.
20. P. Sui, W. Zhang, H. Lin, B. Wang, P. F. Wang, Y. Lin, J. Xu, Y. Cheng and Y. S. Wang, *J. Mater. Chem. C*, 2024, **12**, 15596-15606.
21. Y. Lin, H. Lin, P. F. Wang, J. Xu, Y. Cheng and Y. S. Wang, *Laser Photon. Rev.*,

2024, 2400995.